Iterative 3D-MRF based Decoder for Uncompressed Wireless Video Transmission

Wei-Chih Hung, Wei-Ting Lin, Kuan-Yu Lin, Ping-Cheng Yeh
Graduate Institute of Communication Engineering
National Taiwan University
Taipei, Taiwan

***Abstract*—Due to the emergence of mmWave systems that provide multi-Gbps data rate over 60GHz band, uncompressed video transmission has been considered as a commonly used feature for wireless multimedia transmission over the wireless personal area networks (WPANs). However, mmWaves signals usually have higher attenuation than the conventional low-frequency wireless signals, and therefore supporting transmission in a low SNR condition becomes a challenging problem for such systems. In this paper, we propose a 3D-MRF model and an iterative source-channel decoding method based on the proposed 3D-MRF model for the wireless transmission of uncompressed video. With our proposed iterative decoding structure, the video decoder utilizes the temporal and spatial redundancy among the video frames to jointly decode the received coded bits with the aid of 3D-MRF model. The numerical results show that the proposed method can significantly enhance the video quality in terms of PSNR, even while operating in an extremely low SNR condition.**

***Index Terms*—Markov random fields, iterative source-channel decoding, wireless communication, video signal processing.**

I. Introduction

THE prevalence of video technology make it easy for people to access multimedia services and products such as digital films, video streaming and Internet video communications. Recently, due to the emergence of mmWave systems that provide multi-Gbps data rate over 60GHz band, the video transmission systems using Ultra-wideband (UWB) techniques for the emerging wireless personal area networks (WPANs), such as WirelessHD [1] and Wireless Gigabit Alliance [2], have been developed for better user experience. Different from conventional video streaming systems, these systems require low latency and lossless video quality in order to support features such as display and user interaction. Also, in WPANs the video sources are typically uncompressed HDMI streams from game consoles, PCs and mobile devices. Therefore, with the aid of multi-Gbps data rate over 60GHz band, video sequences are usually transmitted without compression in WPANs video transmission systems [3].

When transmitting over such high-frequency band, wireless signals tends to be much more fragile, compared to the conventional low-frequency wireless signals. In other words, uncompressed video transmission systems over high-frequency band could operate in a low signal-to-noise ratio (SNR) condition, and it might results in damaged video frames. There are several works providing different solutions to enhance the video quality in an uncompressed video transmission system. In [3], pixel partitioning and uncompressed automatic repeat request (UV-ARQ) are proposed. Unequal error protection (UEP), in which different modulation and coding schemes (MCs) are imposed to different pixel levels, is adopted in both [3] and [4]. Furthermore, since in uncompressed video transmission neither the spatial nor the temporal redundancy is removed from the video source, joint source-channel coding (JSCC) [5] can be performed to exploit the redundancy. The question of redundancy reuse is similar to the classic Slepian-Wolf theorem [6], which states that the achievability of the sum-rate of the separated lossless compression of the two correlated sources can be equal to the joint entropy. However, in JSCC, the correlations are not used to compress the sources but used to improve the communication reliability. By combing the side information along with error correction code, a communication system can achieve better performance than the one without utilizing the side information. In [7] and [8], JSCC is used for speech error concealment with the aid of first-order Markov process.

Based on JSCC, iterative source-channel decoding (ISCD) [9]–[13] was developed as a turbo-like [14] decoding structure to exchange the extrinsic information between channel decoder and source decoder, and thus increasing the error robustness of the receiver. In [15], ISCD is used for image transmission with the assumption that each image pixel is constrained by two first-order Markov processes in horizontal and vertical directions. The same model is generalized from 2D to 3D by taking the third temporal first-order Markov process in video into consideration in [16]. In [16], the state transition probability of the first-order Markov process is obtained by off-line statistic data of videos, and the temporal first-order Markov process is formed by assuming a pixel is related to all pixels in the same location within every video frame. A ISCD scheme for image decoding using Markov Random field (MRF) to model the relationship between neighboring pixels is proposed in [17] and [18], where the MRF parameter is estimated in encoder and transmitted to the ISCD decoder which consists a channel decoder and an iterative MRF decoder.

In this paper, we propose an iterative source-channel decoding method for uncompressed video transmission based on a proposed novel 3D-MRF model. The 3D-MRF model is a bit-plane level MRF model which successfully reveals the spatial and temporal redundancy of video sequences. For those video sequences of intense movement, we utilize the motion estimation at the decoder side to precisely locate

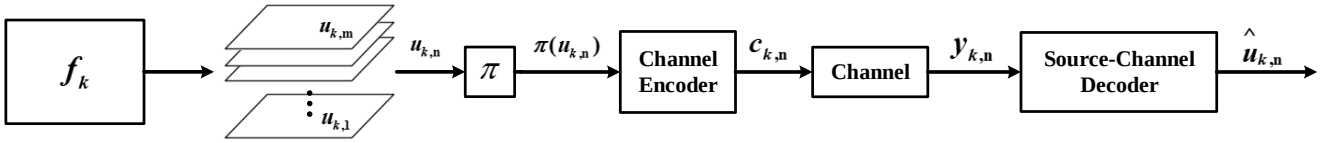

Fig. 1. Wireless video transmission model.

the temporal movement under the block-base view, and thus the temporal redundancy can be fully used by the 3D-MRF. Through the 3D-MRF model, we develop the 3D-MRF based soft-in soft-out (SISO) source decoder. The 3D-MRF based SISO source decoder has much lower complexity than conventional iterative MAP-MRF decoder while still significantly improves the decoding performance. We design an iterative source-channel decoding structure which is capable of jointly estimating the MRF parameters at the receiver, and thus the proposed decoder can automatically adjust the amount of the information exchange according to the decoding video sequence. Also, by adding a single buffer into our decoder structure, the temporal extrinsic information is allowed to propagate throughout the video decoding process. We show that the proposed ISCD method can significantly enhance the video quality in terms of peak signal-to-noise ratio (PSNR). Even under very low SNR condition, the video frames are still maintained in good quality. Furthermore, It is worth noting that our proposed decoding method can cooperate with any existing UEP solutions implemented in the transmitter to provide further improvement in video quality.

The content of this paper is organized as follows. In Section II the transmission system and the wireless channel model are introduced. The 3D-MRF model and the 3D-MRF based SISO source decoder is proposed in Section III. The ISCD decoding method with the joint estimation of the 3D-MRF parameter and motion estimation at the decoder side are shown in Section IV. The extrinsic information transfer (EXIT) chart analysis of the proposed iterative source-channel decoder is provided in Section V. The simulation result is shown in Section VI. Finally the conclusion is made in Section VII.

II. System Model

We consider the wireless video transmission model as depicted in Fig. 1. At time instant τ, a video frame F_k with incremental index k is captured from the video source. The set consisting of the pixels from F_k is denoted as

$$\mathbf{f}_k = \{f_k^{(x,y)} | x \in \{1,..,w\}, y \in \{1,...,h\}\}, \tag{1}$$

where (w,h) are the width and height of the video frame F_k. Each element of $\mathbf{f}_k$ is an m-bit unsigned integer, whose value ranges from 0 to $2^m - 1$. For convenience, the video frame pixels can also be represented in a bit-plane way, where

$$\mathbf{u}_{k,n} = \{u_{k,n}^{(x,y)} = f_k^{(x,y)}(n) | \forall f_k^{(x,y)} \in \mathbf{f}_k\} \tag{2}$$

are the n-th bit-plane of the k-th video frame with $n = 1,...,m$, and $f_k^{(x,y)}(n)$ is the n-th bit of $f_k^{(x,y)}$ ($n = 1$ for the most significant bit (MSB) and $n = m$ for the least significant bit (LSB).) Each bit-plane is scanned into serial bit-sequence and interleaved by the block π in Fig. 1 which is assumed to be a random interleaver. After applying the channel code on interleaved bit sequence, we obtain the channel-coded bit sequence $\mathbf{c}_{k,n} = [c_{k,n}^1, c_{k,n}^2, ..., c_{k,n}^{w \cdot h/R_c}]$ with $w \cdot h$ denoting the total number of bits in a bit-plane and the code rate R_c of the applied channel code. These coded bits are then modulated and passed through an additive white Gaussian noise (AWGN) channel with signal-to-noise ratio (SNR) E_b/N_0. Assuming binary phase shift keying (BPSK) is used, the received signal of $c_{k,n}^i$ can be described by

$$y_{k,n}^i = (2c_{k,n}^i - 1) + z, z \sim Gau(0, \frac{N_0}{2\sqrt{E_s}}), \tag{3}$$

where $Gau(\mu, \sigma^2)$ is the Gaussian distribution with mean μ and variance σ^2. Furthermore, the log-likelihood ratio (LLR) is computed as

$$L(y_{k,n}^i) = \ln[\frac{p(y_{k,n}^i | c_{k,n}^i = 0)}{p(y_{k,n}^i | c_{k,n}^i = 1)}] = 4\frac{E_s}{N_0} y_{k,n}^i, \tag{4}$$

where $p(\cdot)$ is the probability distribution function (p.d.f) of $y_{k,n}^i$. These LLR values are then passed through our proposed 3D-MRF decoder whose output is the estimated source bit sequence $\hat{\mathbf{u}}_{k,n}$.

III. 3D-MRF Model

In this section, we first briefly review the MRF basic property, and then present the proposed 3D-MRF model by defining the spatial and temporal neighborhood relationship among all the bits in a transmitted video sequence. The neighborhood relationship defined by the 3D-MRF model reveals the spatial and temporal redundancy of commonly used video sequences. In our proposed decoding method, the redundancy is exploited by the joint source-channel decoder to enhance the video quality as well as to increase the system robustness.

A. MRF theory

The basic two elements of an MRF are sites and the labels corresponding to those sites. For example, in most image reconstruction MRF applications, a site usually refers to the position/index of a pixel, and the label is usually the corresponding pixel value in that position. For a site denoted as i, the corresponding label q_i which takes value in $\mathcal{Q}$ is assumed to be a realization of the random variable q_i. Let S be a set consisting of multiple sites with size $|S|$. The neighborhood system used to relate each site in S to others is defined as

$$N = \{N_i | \forall i \in S\} \tag{5}$$

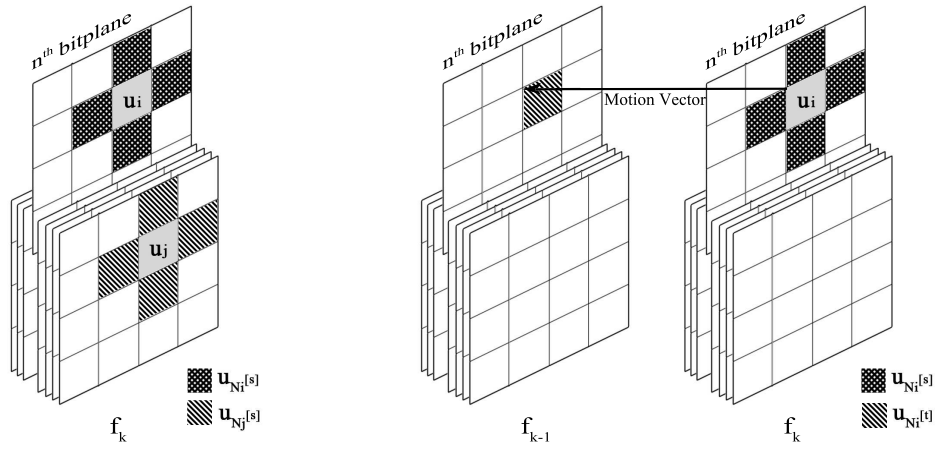

Fig. 2. 3D-MRF model, where 2a presents the spatial neighborhood system, and 2b presents the temporal neighborhood system.

where N_i is defined as the set consisting of an arbitrary site i's neighborhood sites with respect to the neighborhood system. Furthermore, take

$$Q = \{Q_1, Q_2, ..., Q_{|S|}\} \tag{6}$$

as a random field consisting of all the labels of sites in S. A configuration $q = \{q_1, q_2, ...q_{|S|}\} \in \mathcal{Q}^m$ is a joint realization with respect to Q. Given a configuration q, the joint event $\{Q_1 = q_1, Q_2 = q_2, ..., Q_{|S|} = q_{|S|}\}$ is denoted as $Q = q$, and the joint probability $P(Q = q)$ is simply represented by $P(q)$. Q with the neighborhood system N is said to be an MRF if and only if positivity and Markovianity appear in F. The positivity is defined by

$$P(q) > 0, \forall f \in \mathcal{Q}, \tag{7}$$

and the Markovianity says that

$$P(q_i|q_{S-\{i\}}) = P(q_i|f_{N_i}), \tag{8}$$

where $f_{S-\{i\}}$ are the set of labels at all the sites in S except the site i. The positivity as a global property implies that given an arbitrary joint realization (configuration) of L, there is an unique non-zero joint probability for this configuration. In other hands, Markovianity provides the local property of an MRF by saying that a site's label only depends on it's neighborhood's labels. If we specify a set of sites$S$, a neighborhood system N and the conditional probability distribution $P(q_i|q_{N_i})$ of any arbitrary site's label in S, an MRF is uniquely defined.

Gibbs distribution is proved to be an MRF [19] and is widely used in MRF applications. A Gibbs distribution is defined as

$$P(q_i|q_{N_i}) = Z^{-1} \times e^{-U(q_i, q_{N_i})}, \tag{9}$$

where

$$Z = \sum_{q_i \in \mathcal{Q}} e^{-U(q_i, q_{N_i})}, \tag{10}$$

and $U(q_i, q_{N_i})$ is the energy function. For a given configuration q and site i, the energy computed by the energy function $U(q_i, q_{N_i})$ shows the local probability of the configuration q. When the energy value computed by $U(q_i, q_{N_i})$ is high with respect to an arbitrary site i and local configuration $Q_i = q_i$, the local probability $P(q_i|q_{N_i})$ becomes low, and thus the event $Q_i = q_i$ has less chance to appear. If we only consider the first-order neighborhood relationship (i.e., the pairs of sites where each pair is constructed by a site i and one of its neighborhood $i' \in N_i$), the energy function of a Gibbs distribution can be expanded as

$$U(q_i, q_{N_i}) = \sum_{i' \in N_i} V_{(i,i')}(q_i, q_{i'}), \tag{11}$$

where $V_{(i,i')}(q_i, q_{i'})$ is the potential function which computes the potential between (i, i'), and the form of potential function $V_{(i,i')}(\cdot)$ can vary from different (i, i') (e.g., geometry shape, location, ..., etc.).

B. 3D-MRF Model

The proposed 3D-MRF model is a low-level MRF model, linking each bit of a transmitted video frame to it's surrounding bits both in spatial and temporal direction as depicted in Fig. 2. For simplicity, a single bit $u_{k,n}^{(x,y)}$ mentioned in Section II is denoted as u_i, where a single index i comprises the indices (k, n, x, y). Let u_i represent a single site in 3D-MRF. The set composed by the neighborhood sites of u_i can be separated into two subsets as

$$N_i = N_i^{[s]} \cup N_i^{[t]}, \tag{12}$$

where $N_i^{[s]}$ is the spatial neighborhood subset, and $N_i^{[t]}$ is the temporal neighborhood subset.

Regarding the spatial homogeneity, we choose 4 nearest bits in the same bit-plane with u_i to form the spatial two dimensional neighborhood system as illustrated in Fig. 2. Thus, the spatial subset $N_i^{[s]}$ is defined as

$$u_{N_i^{[s]}} = \{u_{k,n}^{(x-1,y)}, u_{k,n}^{(x+1,y)}, u_{k,n}^{(x,y-1)}, u_{k,n}^{(x,y+1)}\}. \tag{13}$$

Furthermore, considering the temporal subset $N_i^{[t]}$, we propose using the decoder-side motion estimation to locate the local

motion vectors between received video frames, which will be detailed in Section IV. Through the local motion vector, a pixel $f_k^{(x,y)}$ at location (x, y) in frame k is related to another pixel $f_{k-1}^{(x',y')}$ at location (x', y') in the previous frame $k-1$, where (x', y') is computed from decoder side motion estimation. As a result, we let those bits in $\mathbf{f}_{k-1}$ which is located by the motion vector becomes the temporal neighborhood sites of bits in $\mathbf{f}_k$ to show the temporal redundancy in the MRF model, and thus the temporal neighborhood subset is

$$u_{N_i^{[t]}} = \{u_{k-1,n}^{(x',y')}, x' = x - v_i^x, y' = y - v_i^y\}, \quad (14)$$

where (v_i^x, v_i^y) is the local motion vector which belongs to u_i.

The reason why we choose each site in 3D-MRF to be represented by a single bit in a bit-plane of a video frame instead of the pixel value from the m-bit pattern is mainly due to the complexity issue. The decoding process chosen by soft decoding is either a maximum likelihood (ML) or maximum *a posteriori* probability (MAP) decision, where both require a number of 2^m probability computation if a m-bit pattern is assumed to be decoded. By using our proposed bit-plane level MRF model, the decoding process is simplified from single decision problem with complexity $O(2^m)$ to m decision problems, where each one is a $0/1$ decision problem and the total complexity is $O(2m)$. Taking $m = 8$ as a common set-up, the decoding complexity of a pixel is 16 times lower than the conventional one, resulting a significant complexity improvement.

The probability of a site u_i conditional on its neighborhood sites in 3D-MRF takes the form

$$P(u_i|u_{N_i}) = Z^{-1} \times e^{-U(u_i,u_{N_i})}, \quad (15)$$

which is a Gibbs distribution as defined in (9). Also, from (10), we obtain Z as

$$Z = \sum_{u_i \in \{0,1\}} e^{-U(u_i,u_{N_i})} \quad (16)$$

$$= e^{-U(u_i=0,u_{N_i})} + e^{-U(u_i=1,u_{N_i})}. \quad (17)$$

The energy function $U(u_i, u_{N_i})$ is the summation of both spatial and temporal neighborhood pairs' potential as

$$U(u_i, u_{N_i}) = \sum_{i' \in N_i^{[s]}} V_c^{[s]}(u_i, u_{i'}) + \sum_{i' \in N_i^{[t]}} V_c^{[t]}(u_i, u_{i'}). \quad (18)$$

By assuming each bit-plane is a piecewise constant surface, we let the potential functions $V_c^{[s]}$ and $V_c^{[t]}$ take the form

$$V_c^{[s]}(u_i, u_{i'}) = \beta_s(1 - \delta(u_i - u_{i'})) \quad (19)$$

and

$$V_c^{[t]}(u_i, u_{i'}) = \beta_t(1 - \delta(u_i - u_{i'})), \quad (20)$$

where $\delta(u)$ is the Dirac delta function, and $\delta(u) = 1$ only when $u = 0$. In other words, for each neighborhood pair $(u_i, u_{i'})$, $i' \in N_i$, if $u_i \neq u_{i'}$, a penalty term is added to the energy function $U(u_i, u_{N_i})$, where the penalty term is β_s or β_t according to whether $u_{i'}$ is a spatial neighborhood site or a temporal one. The penalty coefficient β_s and β_t represent the homogeneity of the transmitted video sequence, where a high value of a penalty coefficient implies that there is a significant similarity between the neighborhood sites in 3D-MRF. In our proposed decoding method, β_s and β_t are estimated from the video content on-the-fly for each frame and bit-plane.

C. 3D-MRF Based SISO Source Decoding

The source decoder based on proposed 3D-MRF model is an SISO decoder, where the inputs and outputs are both LLRs of each bit in the transmitted video sequences. For a single site u_i, the input *a priori* LLR of u_i is denoted as

$$L_i^{(I)} = L_s^{(I)}(u_i) = \ln \frac{P(u_i = 0)}{P(u_i = 1)}. \quad (21)$$

We derive the decoding method through the *a posteriori* probability based on proposed 3D-MRF model. For each site, the *a posteriori* probability output can be represented by the *a posteriori* LLR

$$L_i^{(O)} = \ln \frac{P(u_i = 0|L_i^{(I)}, L_{N_i}^{(I)})}{P(u_i = 1|L_i^{(I)}, L_{N_i}^{(I)})}, \quad (22)$$

where $L_{N_i}^{(I)}$ is the set composed of input *a priori* LLRs of N_i which is the neighborhood of u_i in proposed 3D-MRF model. From Bayes' theorem and the fact that $P(u_i) = 1/2$ and $\ln(P(u_i = 0)/P(u_i = 1)) = 0$ when the probability is not conditional on the input *a priori* information $L_i^{(I)}$, (22) can be modified as

$$L_i^{(O)} = \ln \frac{P(u_i = 0, L_i^{(I)}, L_{N_i}^{(I)})}{P(u_i = 1, L_i^{(I)}, L_{N_i}^{(I)})}$$

$$= \ln \frac{P(L_i^{(I)}|u_i = 0, L_{N_i}^{(I)})}{P(L_i^{(I)}|u_i = 1, L_{N_i}^{(I)})} + \ln \frac{P(u_i = 0|L_{N_i}^{(I)})}{P(u_i = 1|L_{N_i}^{(I)})}. \quad (23)$$

Also, since that $L_i^{(I)}$ and $L_{N_i}^{(I)}$ are conditionally independent when u_i is given, (23) is further derived as

$$L_i^{(O)} = \ln \frac{P(u_i = 0|L_i^{(I)})}{P(u_i = 1|L_i^{(I)})} + \ln \frac{P(u_i = 0|L_{N_i}^{(I)})}{P(u_i = 1|L_{N_i}^{(I)})}, \quad (24)$$

where the first term are simply $L_i^{(I)}$ itself, and the second term is the probabilities conditional on N_i described from the 3D-MRF model. However, for each site in N_i, we have only their LLRs instead of the exact value of u_{N_i}, and thus the conditional probability in (15) of 3D-MRF model cannot be directly used in the derivation. In conventional MAP-MRF decoding method, this problem is usually solved by a iterative process, where in each iteration the $\hat{u}_{N_i}$ estimated from L_{N_i} is used to derive the conditional probability of u_i, and thus imposes computation complexity. We propose a novel solution which can exploit the uncertainty of N_i with a low computation overhead at the same time. We modify the conditional probability of u_i based on the expectation of the energy function $U(u_i, u_{N_i})$ over L_{N_i} as

$$P(u_i|L_{N_i}) = Z^{-1} \times e^{E[U(u_i,u_{N_i})|L_{N_i}]}, \quad (25)$$

where $E[\cdot]$ is the expectation function based on a given probability distribution. From (18), the expectation of energy

function is

$$E[U(u_i,u_{N_i})|L_{N_i}] = \sum_{i'\in N_i^{[s]}} E[V_c^{[s]}(u_i,u_{i'})|L_{i'}] + \sum_{i'\in N_i^{[t]}} E[V_c^{[t]}(u_i,u_{i'})|L_{i'}], \quad (26)$$

Furthermore, the potential functions in (26) can be simplified by taking expectation on each neighborhood pair's potential in (19) and (20) over the LLR values as

$$E[V_c^{[s]}(u_i,u_{i'})|L_{i'}] = \beta_s(P(u_{i'} \neq u_i|L_{i'})) \quad (27)$$

and

$$E[V_c^{[t]}(u_i,u_{i'})|L_{i'}] = \beta_t(P(u_{i'} \neq u_i|L_{i'})),, \quad (28)$$

where β_s and β_t are the 3D-MRF parameter of the decoding video. By combining (22)-(28), the *a posteriori* LLR in (22) can be shown as

$$L_i^{(O)} = \ln\frac{P(u_i=0|L_{N_i})}{P(u_i=1|L_{N_i})} + \ln\frac{P(u_i=0|L_i)}{P(u_i=1|L_i)} \quad (29)$$

$$= \sum_{i'\in N_i^{[s]}} \beta_s(P(u_{i'}=1|L_{i'}) - P(u_{i'}=0|L_{i'})) + \sum_{i'\in N_i^{[t]}} \beta_t(P(u_{i'}=1|L_{i'}) - P(u_{i'}=0|L_{i'})) + L_i, \quad (30)$$

where the first term and second term correspond to the extrinsic information of spatial part and temporal part in 3D-MRF respectively, and the third term is simply the *a priori* information. Thus, we reformulate the 3D-MRF decoding output as

$$L_i^{(O)} = L_i^{(E,s)} + L_i^{(E,t)} + L_i^{(I)}, \quad (31)$$

where $L_i^{(E,s)}$ and $L_i^{(E,t)}$ are the first term and second term in (30). It shows that we can separately compute the extrinsic information $L_i^{(E,s)}$ and $L_i^{(E,t)}$ solely from the LLR of u_i's neighborhood without L_i involved, which is convenient for the iterative source-channel decoding discussed in Section IV.

IV. Iterative Channel-Source Decoding Algorithm

In this section, the iterative channel-source decoding algorithm based on the proposed 3D-MRF is presented. The iterative decoder structure is shown in Fig. 3, where the iterative decoding of two consecutive received frames is performed by the extrinsic information exchange between channel decoder and source decoder, as well as between two consecutive received video frames. In the following subsections, we firstly introduce the decoder side motion estimation, which is used to locate the temporal neighborhood. Then the 3D-MRF parameter estimation is derived using a least square error solution. Along with the 3D-MRF based SISO source decoding proposed in III-C, the iterative decoding flow is finally detailed in IV-C.

A. Decoder Side Motion Estimation

In the proposed 3D-MRF model, the temporal neighborhood system aims to describe the temporal redundancy of the commonly used video sequences. Though the nearby video frames usually have high similarity, the movement of pixels should not be ignored. In the conventional video compression, motion estimation is the widely-used tool to locate the movement between the video frames, and thus the temporal redundancy can be removed in the video compression process. Also, in the distributed video coding (DVC) [20], the motion estimation is implemented in the decoder side to generate the side information of a Winer-Ziv frame [22], which is an interpolation of received intra-coded frame. Therefore, we select the decoder side motion estimation as the tool to describe the temporal redundancy.

However, different from the conventional video compression and DVC, in our work, the decoder side motion estimation is used to locate the temporal neighborhood relationships in proposed 3D-MRF model mentioned in III-B between received uncompressed video frames. In our decoder side motion estimation, a received and decoded video frame $\hat{\mathbf{f}}_k$ is divided into several macro-blocks (MB), each of whom consists of several pixels in $\hat{\mathbf{f}}_k$. For an i-th MB in $\hat{\mathbf{f}}_k$ denoted as $\mathbf{b}_{k,i}$, it searches for a motion vector $v_{k,i} = (v_{k,i}^x, v_{k,i}^y)$ such that

$$v_{k,i} = \underset{v_{k,i}^x, v_{k,i}^y \in \{-d,d\}}{\arg\min} \sum_{\hat{f}_k^{(x,y)} \in \mathbf{b}_{k,i}} c(\hat{f}_k^{(x,y)}, \hat{f}_{k-1}^{(x-v_{k,i}^x, y-v_{k,i}^y)}), \quad (32)$$

where d is the search range, and $c(f,f')$ is the cost function between two pixels f and f'. We use mean absolute deviation (MAD) as the cost function, where

$$c(f,f') = |f-f'|, \quad (33)$$

where $|\cdot|$ is the absolute value. As a result, for each pixel $\hat{f}_k^{x,y} \in \mathbf{b}_{k,i}$, there is a corresponding pixel in the previous frame $\hat{\mathbf{f}}_{k-1}$ indicated by the motion vector $v_{k,i}$. After acquiring the local motion vector for a pixel $\hat{f}_k^{x,y}$, the temporal neighborhood site $N_i^{[t]}$ of a bit $\hat{u}_{k,n}^{(x,y)}$, which is the n-th bit of $\hat{f}_k^{x,y}$, is located through (14), where the motion vector is $v_{k,i}$. It is worth noting that the same motion vector $v_{k,i}$ located by $\hat{f}_k^{x,y}$ is used for each element of the set $\{\hat{u}_{k,n}^{(x,y)} | n = 1...m\}$.

B. Parameter Estimation

In this subsection, the parameter estimation of β_s and β_t, as "Parameter Estimator" illustrated in Fig. 3, is performed by the least-square fit solution first proposed by [23]. Consider the conditional probability $P(u_i|u_{N_i})$ in (15) where the left-hand side is modified by Bayes' theorem as

$$\frac{P(u_i,u_{N_i})}{P(u_{N_i})} = \frac{e^{-U(u_i,u_{N_i})}}{e^{-U(0,u_{N_i})} + e^{-U(1,u_{N_i})}}. \quad (34)$$

Rearranging the above equation, we yield

$$\frac{e^{-U(0,u_{N_i})} + e^{-U(1,u_{N_i})}}{P(u_{N_i})} = \frac{e^{-U(u_i,u_{N_i})}}{P(u_i,u_{N_i})}. \quad (35)$$

Note that the left-hand side in (35) is independent to whether u_i is 0 or 1. Therefore, substitute $u_i = 0$ and $u_i = 1$ into the

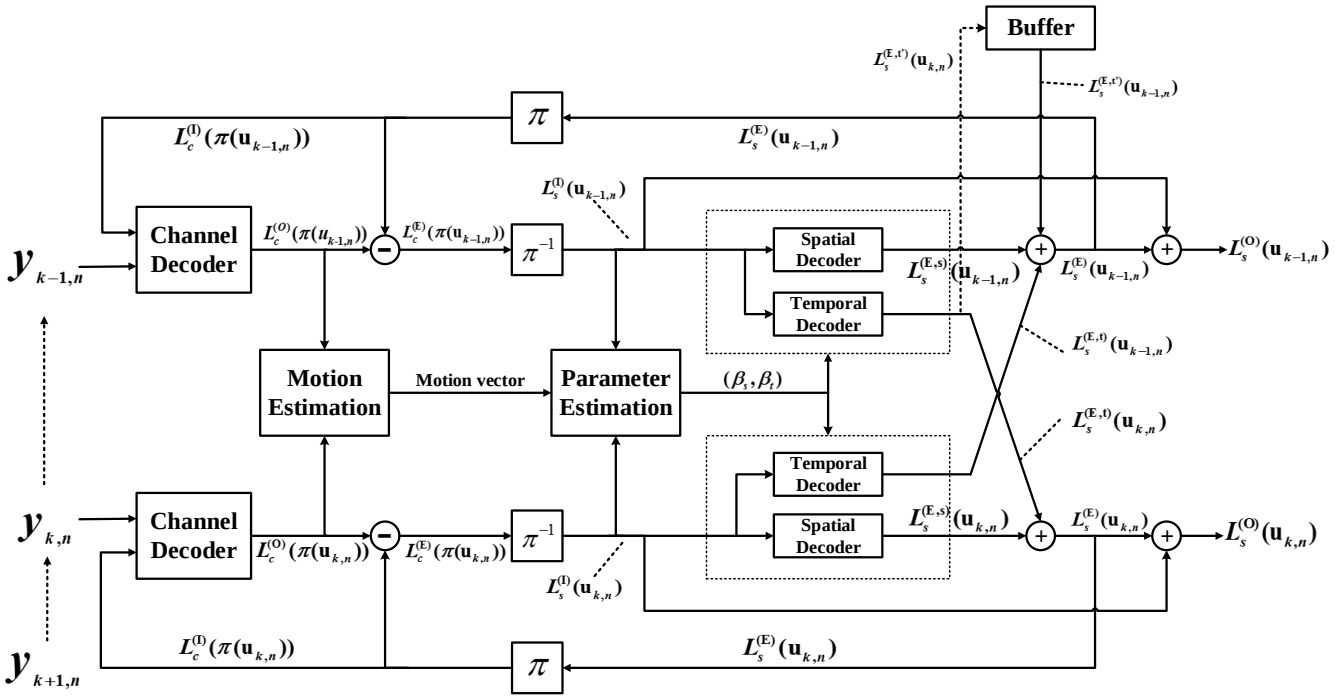

Fig. 3. 3D-MRF based Iterative source-channel decoder structure.

right-hand side of (35) and link them through the left-hand side of (35), we have

$$\frac{e^{-U(u_i=0,u_{N_i})}}{P(u_i=0,u_{N_i})}=\frac{e^{-U(u_i=1,u_{N_i})}}{P(u_i=1,u_{N_i})}. \tag{36}$$

Again we rearrange and take the logarithm of two sides in (36) as

$$\ln(\frac{e^{-U(u_i=0,u_{N_i})}}{e^{-U(u_i=1,u_{N_i})}})=\ln(\frac{P(u_i=0,u_{N_i})}{P(u_i=1,u_{N_i})}). \tag{37}$$

Substitute (19) and (20) into the left-hand side of (37), and we have

$$\beta_s x_i^{[s]}+\beta_t x_i^{[t]}=y_i, \tag{38}$$

where

$$x_i^{[s]}=\#\{u_{N_i^{[s]}}=0\}-\#\{u_{N_i^{[s]}}=1\}, \tag{39}$$

$$x_i^{[t]}=\#\{u_{N_i^{[t]}}=0\}-\#\{u_{N_i^{[t]}}=1\}, \tag{40}$$

$$and y_i=\ln(\frac{P(u_i=0,u_{N_i})}{P(u_i=1,u_{N_i})}). \tag{41}$$

Note that (38) is a linear equation with respect to β_s and β_t, which implies that β_s and β_t can be obtained from linear equations once we have $P(u_i,u_{N_i})$. This problem is solved by histogram technique. Assume we have a sample set $\mathbf{u}$ consisting of multiple sites in 3D-MRF with size $|\mathbf{u}|$. Using histogram technique, the local joint probability can be expressed as

$$P(u_i,u_{N_i})=\frac{H(u_i,u_{N_i})}{|\mathbf{u}|}, \tag{42}$$

where $H(u_i,u_{N_i})$ is the histogram count of the local configuration (u_i,u_{N_i}) occurs in $\mathbf{u}$, and therefore

$$y_i=\ln(\frac{H(u_i=0,u_{N_i})}{H(u_i=1,u_{N_i})}). \tag{43}$$

To obtain β_s and β_t from the sample set $\mathbf{u}$, we denote $x_i^{[s]}$ and $x_i^{[t]}$ of the sample set $\mathbf{u}$ as two column vectors, and we obtain the linear equations

$$\begin{pmatrix} x_1^{[s]} & x_1^{[t]} \\ x_2^{[s]} & x_2^{[t]} \\ \vdots & \vdots \\ x_{|\mathbf{u}|}^{[s]} & x_{|\mathbf{u}|}^{[t]} \end{pmatrix}\begin{pmatrix}\beta_s\\ \beta_t\end{pmatrix}=\begin{pmatrix} y_1\\ y_2\\ \vdots\\ y_{|\mathbf{u}|}\end{pmatrix}, \tag{44}$$

which is an overdetermined system simply denoted as

$$\mathbf{X}\begin{pmatrix}\beta_s\\ \beta_t\end{pmatrix}=\mathbf{Y}. \tag{45}$$

Thus, β_s and β_t can be estimated with a conventional least-square solution :

$$\begin{pmatrix}\beta_s\\ \beta_t\end{pmatrix}=\mathbf{X}^{\dagger}\mathbf{Y}, \tag{46}$$

where $\mathbf{X}^{\dagger}$ is the Moore-Penrose pseudoinverse of matrix $\mathbf{X}$. It is worth noting that the parameter estimation mentioned here is performed with each bit-plane separately.

C. Iterative Process

With the estimator and the extrinsic information equation, the iterative decoding process is performed with the following steps as shown in Fig. 3:

1) Initialize the *a prior* information of two SISO channel decoder by setting all bits to be equiprobable (i.e., set $L_c^{(I)}$ to be all zero.)
2) For each frame, pass the received signals $\mathbf{y}$ with *a priori* information $L_c^{(I)}$ through the SISO channel decoders, and get the output LLR values $L_c^{(O)}$. The extrinsic information LLRs $L_c^{(E)}$ are computed through subtracting the *a priori* LLRs $L_c^{(I)}$ from the output LLRs $L_c^{(O)}$.
3) Compute the local motion vector from the channel decoded and deinterleaved two consecutive frames $\hat{\mathbf{f}}_k$ and $\hat{\mathbf{f}}_{k-1}$ using (32), and locate the temporal neighborhood of each site using (14).
4) Estimate the 3D-MRF parameter β_s and β_t for each bit-plane using (46) mentioned in Section IV-B.
5) Pass the deinterleaved channel output extrinsic LLRs as the input *a priori* LLRs $L_s^{(I)}$ to the 3D-MRF based SISO source decoder based on the 3D-MRF parameter estimated in step 4. In the source decoder, use (30) to obtain the spatial and temporal extrinsic information, denoted as $L_s^{(E,s)}$ and $L_s^{(E,t)}$, respectively.
6) Obtain the joint source extrinsic LLRs $L_s^{(E)}$ of frame $k-1$. Sum up the spatial extrinsic information $L_s^{(E,s)}$, the temporal extrinsic information $L_s^{(E,t)}$, and the buffered temporal extrinsic information $L_s^{(E,t')}$ of previous decoding cycle, which is actually the temporal information from frame $k-2$.
7) Obtain the joint source extrinsic LLRs $L_s^{(E)}$ of frame k by summing up the spatial extrinsic information $L_s^{(E,s)}$ and the temporal extrinsic information $L_s^{(E,t)}$. Buffer the temporal extrinsic information $L_s^{(E,t)}$ as $L_s^{(E,t')}$ if it is the last iteration.
8) Pass the extrinsic information of source decoder $L_s^{(E)}$ through the interleavers to acquire the *a prior* information $L_c^{(I)}$ for channel decoder, which is used for the next iteration.
9) If not the final iteration, go to step 2. Otherwise, pass the output LLR values of all bit planes, which is the summation of $L_s^{(I)}$ and $L_s^{(E)}$, denoted as $L^{(O)}$, through a simple sign detector and combine them to form the decoded frames.

The iterative decoder design follows few basic ideas. First, to avoid the overlapping information, only the extrinsic information is exchanged between channel and source decoders. Second, since the goal of the decoder side motion estimation is to locate the temporal sites in 3D-MRF, it is naturally to use the full *a posteriori* information instead of the extrinsic information as the input of motion estimation. Third, the temporal information can be both obtained from the previous and the next frame. However, the complexity and latency would dramatically increase if we decoding 3 frames simultaneously. Therefore, we design a consecutive decoding process to keep the temporal extrinsic information propagating from frame to frame without the increase of complexity and latency. We put a buffer in the decoder structure to buffer the temporal extrinsic information (step 7) from the previous frame, and thus it could be used (step 6) to improve the source decoding when the next video frame is received.

The iterative source-channel decoder shown in Fig. 3 have the properties of both serial concatenated codes (SCCC) and parallel concatenated codes (PCCC). In the serial direction, the 3D-MRF spatial redundancy can be seen as an outer code in SCCC, and the channel code, which encodes the video frames generated by the 3D-MRF redundancy, is seen as the inner code in SCCC. Thus, the extrinsic information exchanging process between the 3D-MRF based spatial decoder and the channel decoder in the proposed ISCD process is just like the conventional iterative decoding of SCCC. In the parallel direction, the temporal redundancy of consecutive video frames is exploited by the 3D-MRF temporal decoder, where the previous frame and the next frame of the current decoding frame can provide the parallel extrinsic information to the 3D-MRF temporal decoder, acting like the conventional PCCC iterative decoder. Furthermore, by the consecutive decoding depicted in our proposed ISCD decoder structure, this parallel information provided by the nearby frames can propagate throughout the decoding process and thus improve the information gain as well as decoding performance. Consequently, the iterative source-channel decoding base on the 3D-MRF model combine the spatial (serial) and temporal (parallel) extrinsic information and therefore significantly enhance the video decoding quality.

V. EXIT Charts Analysis

The extrinsic information transfer chart (EXIT chart) [24] is an useful tool allowing us to analyze the information exchanging behavior of the iterative decoder. The relationship between input LLRs and output LLRs of an SISO decoder can be visualized in EXIT chart in terms of the mutual information between the LLRs and the transmitted bit sequence.

A. Mutual Information Measurement

Assuming the transmitted bit sequence $\mathbf{u}$ with size $|\mathbf{u}|$ are equipropable ($p(u_i) = 1/2$), the mutual information between $\mathbf{u}$ and the decoder output LLRs denoted by $\mathbf{L}$ is measured by

$$I(\mathbf{L};\mathbf{u}) = 1 - \sum_{i=1}^{|\mathbf{u}|} \log_2(1 + e^{-u_i \cdot L_i}). \tag{47}$$

Therefore, the mutual information between the transmitted bit sequence and the input/output LLRs of channel/source decoder are

$$I_c^{(I)} = I(L_c^{(I)}(\pi(\mathbf{u})), \pi(\mathbf{u})), \tag{48}$$
$$I_c^{(E)} = I(L_c^{(E)}(\pi(\mathbf{u})), \pi(\mathbf{u})), \tag{49}$$
$$I_s^{(I)} = I(L_s^{(I)}(\mathbf{u}), \mathbf{u}), \tag{50}$$
$$I_s^{(E)} = I(L_s^{(E)}(\mathbf{u}), \mathbf{u}), \tag{51}$$

where the terms $I_c^{(I)}$ and $I_s^{(I)}$ represent the average *a prior* information fed into the channel decoder and source decoder respectively. Similarly, $I_c^{(E)}$ and $I_s^{(E)}$ represent the average extrinsic information generated by the channel decoder and source decoder. From this point of view, the output extrinsic information of an SISO decoder can be seen as a function of the input *a priori* information. As a consequence, by adding Gaussian noise with different energy levels to the LLR

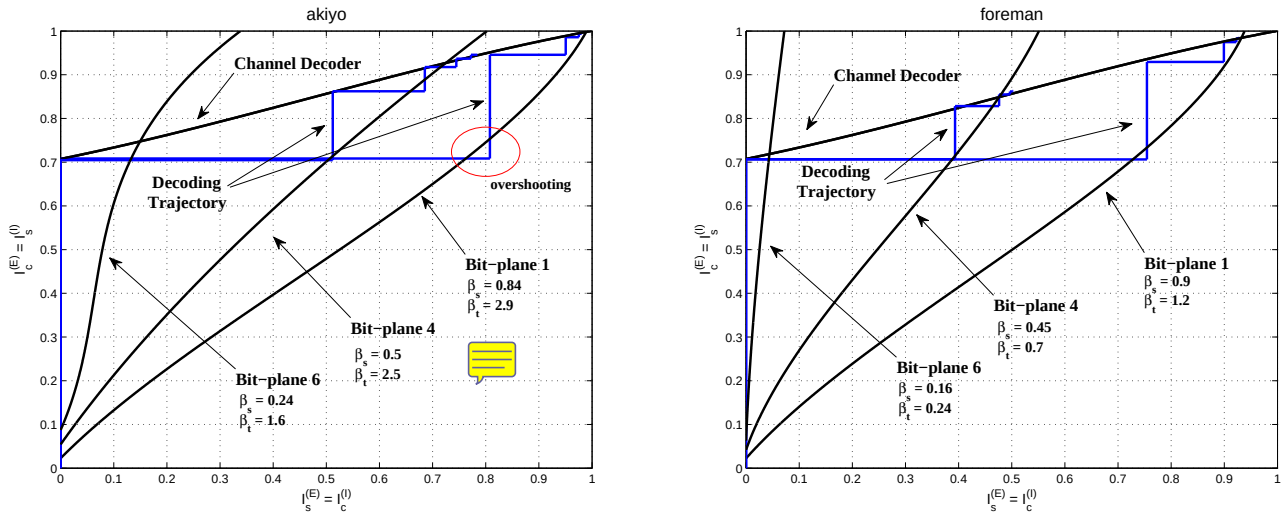

(a) (b)

Fig. 4. EXIT charts of proposed ISCD method using the "akiyo" and the "foreman" sequences with SNR equals 0.

generated by the original transmitted signal and fed it into the SISO decoder, we can measure the decoding function with input $I^{(I)}$ and output $I^{(E)}$ using (47).

Note that $L_c^{(E)}(\pi(\mathbf{u}))$ yields $L_s^{(I)}(\mathbf{u})$ by passing though an deinterleaver, indicating that $I_c^{(E)}$ is actually used as $I_s^{(I)}$ at the source decoder input. Likewise, $I_s^{(E)}$ is used as $I_c^{(I)}$ at the input of channel decoder. Therefore, we can plot these information and the iterative decoding process in a single 2-D graph, where the x-axis is $I_c^{(I)}$ as well as the $I_s^{(E)}$, and the y-axis is $I_c^{(E)}$ and $I_s^{(I)}$.

B. EXIT Chart of 3D-MRF based ISCD Decoder

Fig. 4 shows the EXIT charts of the proposed iterative decoder, where two video sequences and three bit-planes out of eight are presented. Since the decoding performance of the 3D-MRF based decoder is dependent on the video content, given a bi-plane level, the source decoder curve is varying among different video sequences. As a result, in Fig. 4 we observe that the source decoder performance of any bit-plane in"foreman" sequences is better (i.e., the $I_s^{(E)}$ is higher when $I_s^{(I)}$ is fixed) than "akiyo" sequence, indicating that the spatial and temporal redundancy of "akiyo" sequence is more than that of "foreman" sequence. In fact, the decoding performance directly links to the 3D-MRF parameters (β_s, β_t), where the higher values imply the higher correlation between spatial and temporal neighborhood in the video sequence, resulting in better decoding performance. Also, the source decoding performance significantly decreases from MSB to LSB as shown in Fig. 4. Similarly, it is because the higher bit-plane (towards MSB) naturally have the higher homogeneity than the lower bit-plane, and thus the higher bit-plane have the better decoding performance.

C. Overshooting Effect

The difference between the mutual information between each step can be viewed as the information gain coming from the other decoder. By actually measuring the mutual information at each step of the iterative decoding, the decoding trajectory is plotted in Fig. 4, indicating the actual information exchange behavior between the channel decoder and source decoder. For conventional iterative decoding such as turbo decoding, the decoding trajectory is supposed to fit the decoding function curve. However, the "over-shooting" effect, where the extrinsic information generated by the source decoder exceeds the source decoder's decoding curve, appears in Fig. 4.

The reason of "over-shooting" effect discussed in [25] and [26] is similar to our case. During the iterative decoding process, a local area in a video frame with higher homogeneity benefits from the 3D-MRF based decoding more, resulting in that the information gain is actually uneven among all the decoding bits. Since the decoding function curve in the EXIT charts is measured by evenly adding noise to the input LLRs, it causes the mismatch between the decoding trajectory and the decoding function curve. Hence, it appears that the actual decoding performance in terms of information gain and iteration numbers of the source decoder is better than the performance predicted by the decoding function curve.

VI. Experimental Results

We evaluate the proposed iterative source-channel decoding by comparing the direct decoding of convolutional code with the decoder structures as shown in Fig. 3. We use the recursive systematic convolution code which has the generator matrix

$$\mathbf{G}(D) = \begin{bmatrix} 1 & \frac{1+D^2}{1+D+D^2} \end{bmatrix} \tag{52}$$

as the channel correction code, and two different random interleavers are used every other frame. The wireless signals are modulated by BPSK, and the channel noise is assumed to be AWGN. BCJR [27] is used as the soft-in soft-out channel decoder. The iteration count is set to br 3 for all received frames. The evaluation metric is peak signal-to-noise ratio

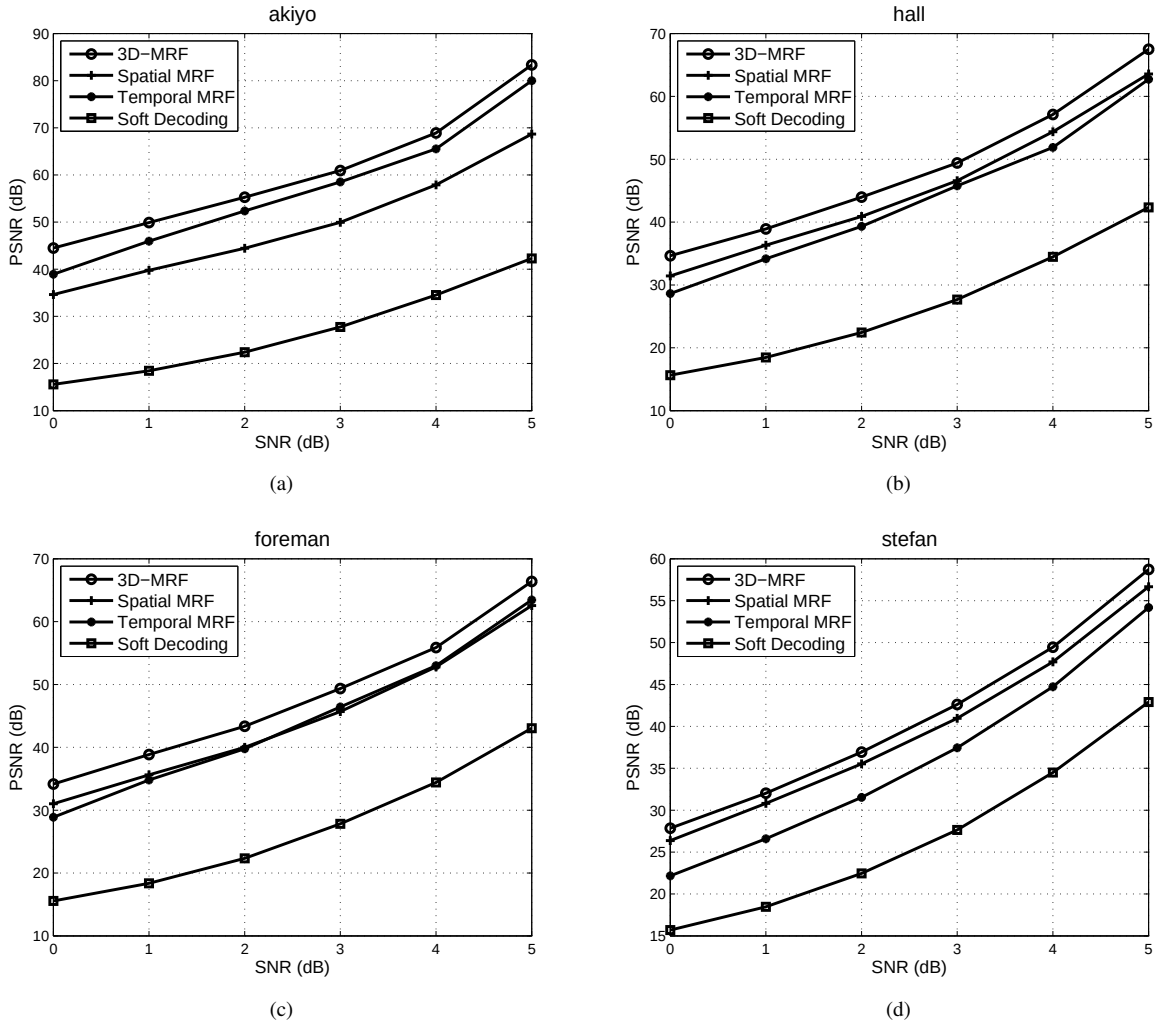

Fig. 5. PSNR gain of proposed decoding method based on 3D-MRF model, where "Spatial MRF" and "Temporal MRF" denotes the decoding gain achieving by solely using the extrinsic information provided by the spatial and temporal decoder respectively, and "Soft decoding" is the BCJR decoding.

(PSNR). For a 8-bit per pixel decoded video frame, the PSNR is represented as

$$PSNR = 20log_{10}(\frac{255}{\sqrt{\frac{1}{w \cdot h}\sum_{i=0}^{w \cdot h}(f_i - \hat{f}_i)^2}}), \qquad (53)$$

where f_i is the pixel value of source video frame, and $\hat{f}_i$ is the decoded pixel value at the receiver. $w \cdot h$ is equal to the total number in a video frame.

We use four video sequences to test our proposed method. These video sequences are composed of gray images with dimension 352×288 pixels, and 8 bits are used to present a pixel. The first 30 video frames are used to evaluate our proposed method. The first sequence is the "akiyo" sequence, in which the human facial expression and body movement present. The second sequence is the "hall" sequence, where there are two objects moving. The hird sequence is the "foreman" sequence, where there is a camera pan movement and apparent facial expression. The forth sequence is the "stefan" sequence, where the faster camera and object movement present. These four video sequences have the common video content, which can test our proposed method in an objective way.

The PSNR gain of our proposed scheme is significant as shown in Fig. 5. It is because that the bit planes homogeneity is increasing from LSBs to MSBs, and the MSBs have the most significant influence on the perceptual qualities as well as PSNR while LSBs have the least. Therefore, the proposed decoding method benefits from the much better correction ability for the more important data. In other words, the UEP is achieved with the inherent image properties. Note that the proposed scheme can still cooperate with other conventional UEP to further improving the video quality. The PSNR gain in motionless video sequences such as "akiyo" is greater than sequences with more movement such as "stefan", since the former has much larger temporal redundancy than the latter one. Nevertheless, the PSNR gain provided by our decoding method for video sequence with intense movement is still quite apparent due to the decoder side motion estimation which exploits the temporal redundancy in these video sequences.

Also, it is worth noting that even in an extremely low SNR condition (e.g., 1 or 0), the PSNR gains generated by joint multi-frame decoding method are 10dB higher than the original soft decoding except for the "stefan" sequence, which

has the strongest camera and object movement among our test video sequences and still has a 5dB PSNR gain in such low SNR condition.

VII. Conclusion

In this work, we have proposed an iterative source-channel decoding method for uncompressed video transmission based on our novel 3D-MRF model. By our proposed 3D-MRF model, one can describe the temporal and spatial redundancy in the transmitted video sequences in a simple bit-plane view. Firstly, based on the 3D-MRF model, we have developed the 3D-MRF based SISO source decoding algorithm which exploits the soft information in the received bit sequence without iterative process. Also, we estimate the 3D-MRF parameter at decoder side to automatically adjust the information shared between the decoded bit sequence without the aid from the encoder. As a consequence, combing the source decoding and the parameter estimation of the 3D-MRF model, we have designed the iterative source-channel decoder scheme. In the proposed ISCD scheme, the extrinsic information is exchanged between the 3D-MRF source decoder and channel decoder, and we design a consecutive decoding structure which propagates the temporal information between video frames.

The numerical results have shown that our proposed method can significantly enhance the video quality in terms of PSNR. Even when intense camera and object movement present, the PSNR gain is still quite remarkable. Furthermore, while the system is operating in an extremely low SNR condition, the video quality is still in good quality. As a result, our proposed scheme successfully enhances the quality and robustness of the wireless transmission of uncompressed video.

Acknowledgment

The authors would like to thank...

References

[1] "WirelessHD," http://www.wirelesshd.org/.
[2] "Wireless Gigabit Alliance," http://www.wigig.org/.
[3] H. Singh, J. Oh, C. Kweon, X. Qin, H. Shao, and C. Ngo, "A 60 GHz wireless network for enabling uncompressed video communication," *Communications Magazine, IEEE*, vol. 46, no. 12, pp. 71–78, 2008.
[4] S. Hong and W. Lee, "Flexible unequal error protection scheme for uncompressed video transmission over 60ghz multi-gigabit wireless system," in *Computer Communications and Networks (ICCCN), 2011 Proceedings of 20th International Conference on*. IEEE, 2011, pp. 1–6.
[5] K. Sayood and J. Borkenhagen, "Use of residual redundancy in the design of joint source/channel coders," *Communications, IEEE Transactions on*, vol. 39, no. 6, pp. 838–846, 1991.
[6] D. Slepian and J. Wolf, "Noiseless coding of correlated information sources," *Information Theory, IEEE Transactions on*, vol. 19, no. 4, pp. 471–480, 1973.
[7] J. Hagenauer, "Source-controlled channel decoding," *Communications, IEEE Transactions on*, vol. 43, no. 9, pp. 2449–2457, 1995.
[8] T. Fingscheidt and P. Vary, "Softbit speech decoding: a new approach to error concealment," *Speech and Audio Processing, IEEE Transactions on*, vol. 9, no. 3, pp. 240–251, 2001.
[9] N. Gortz, "Iterative source-channel decoding using soft-in/soft-out decoders," in *Information Theory, 2000. Proceedings. IEEE International Symposium on*, 2000, pp. 173–.
[10] T. Hindelang, T. Fingscheidt, N. Seshadri, and R. Cox, "Combined source/channel (de-)coding: can a priori information be used twice?" in *Information Theory, 2000. Proceedings. IEEE International Symposium on*, 2000, pp. 266–.
[11] M. Adrat, P. Vary, and J. Spittka, "Iterative source-channel decoder using extrinsic information from softbit-source decoding," in *Acoustics, Speech, and Signal Processing, 2001. Proceedings. (ICASSP '01). 2001 IEEE International Conference on*, vol. 4, 2001, pp. 2653–2656 vol.4.
[12] N. Gortz, "On the iterative approximation of optimal joint source-channel decoding," *Selected Areas in Communications, IEEE Journal on*, vol. 19, no. 9, pp. 1662–1670, 2001.
[13] M. Adrat and P. Vary, "Iterative source-channel decoding: Improved system design using exit charts," *EURASIP Journal on Advances in Signal Processing*, vol. 2005, no. 6, p. 178541, 2005. [Online]. Available: http://asp.eurasipjournals.com/content/2005/6/178541
[14] C. Berrou, A. Glavieux, and P. Thitimajshima, "Near shannon limit error-correcting coding and decoding: Turbo-codes. 1," in *Communications, 1993. ICC 93. Geneva. Technical Program, Conference Record, IEEE International Conference on*, vol. 2. IEEE, 1993, pp. 1064–1070.
[15] J. Kliewer and N. Gortz, "Iterative source-channel decoding for robust image transmission," in *Acoustics, Speech, and Signal Processing (ICASSP), 2002 IEEE International Conference on*, vol. 3, 2002, pp. III–2173–III–2176.
[16] Y. Huo, C. Zhu, and L. Hanzo, "Spatio-temporal iterative source-channel decoding aided video transmission," *Vehicular Technology, IEEE Transactions on*, vol. 62, no. 4, pp. 1597–1609, 2013.
[17] J. Kliewer, N. Gortz, and A. Mertins, "On iterative source-channel image decoding with markov random field source models," in *Acoustics, Speech, and Signal Processing, 2004. Proceedings. (ICASSP '04). IEEE International Conference on*, vol. 4, 2004, pp. iv–661–iv–664 vol.4.
[18] J. Kliewer, N. Goertz, and A. Mertins, "Iterative source-channel decoding with markov random field source models," *Signal Processing, IEEE Transactions on*, vol. 54, no. 10, pp. 3688–3701, 2006.
[19] J. Besag, "Spatial interaction and the statistical analysis of lattice systems," *Journal of the Royal Statistical Society. Series B (Methodological)*, pp. 192–236, 1974.
[20] B. Girod, A. Aaron, S. Rane, and D. Rebollo-Monedero, "Distributed video coding," *Proceedings of the IEEE*, vol. 93, no. 1, pp. 71–83, 2005.
[21] A. Wyner and J. Ziv, "The rate-distortion function for source coding with side information at the decoder," *Information Theory, IEEE Transactions on*, vol. 22, no. 1, pp. 1–10, 1976.
[22] A. Aaron, R. Zhang, and B. Girod, "Wyner-ziv coding of motion video," in *Signals, Systems and Computers, 2002. Conference Record of the Thirty-Sixth Asilomar Conference on*, vol. 1, 2002, pp. 240–244 vol.1.
[23] H. Derin and H. Elliott, "Modeling and segmentation of noisy and textured images using gibbs random fields," *Pattern Analysis and Machine Intelligence, IEEE Transactions on*, vol. PAMI-9, no. 1, pp. 39–55, 1987.
[24] S. Ten Brink, "Convergence behavior of iteratively decoded parallel concatenated codes," *Communications, IEEE Transactions on*, vol. 49, no. 10, pp. 1727–1737, 2001.
[25] M. Adrat, M. Antweiler, L. Schmalen, P. Vary, and T. Clevorn, "On the overshooting effect in exit charts of iterative source-channel decoding," in *Communications (ICC), 2010 IEEE International Conference on*, 2010, pp. 1–5.
[26] L. Schmalen, M. Adrat, T. Clevorn, and P. Vary, "Exit chart based system design for iterative source-channel decoding with fixed-length codes," *Communications, IEEE Transactions on*, vol. 59, no. 9, pp. 2406–2413, 2011.
[27] L. Bahl, J. Cocke, F. Jelinek, and J. Raviv, "Optimal decoding of linear codes for minimizing symbol error rate (corresp.)," *Information Theory, IEEE Transactions on*, vol. 20, no. 2, pp. 284–287, 1974.

PLACE PHOTO HERE

Michael Shell Biography text here.

John Doe Biography text here.

Jane Doe Biography text here.